Eur. Phys. J. B **40**, 427–431 (2004)
DOI: 10.1140/epjb/e2004-00274-x

THE EUROPEAN PHYSICAL JOURNAL B

Dynamics of the first-order magnetostructural transition in $Gd_5(Si_xGe_{1-x})_4$

F. Casanova[1], A. Labarta[1,a], X. Batlle[1,b], E. Vives[2], J. Marcos[2], L. Mañosa[2], and A. Planes[2]

[1] Departament de Física Fonamental, Universitat de Barcelona, Diagonal 647, 08028 Barcelona, Catalonia, Spain
[2] Departament d'Estructura i Constituents de la Matèria, Universitat de Barcelona, Diagonal 647, 08028 Barcelona, Catalonia, Spain

Received 30 January 2004 / Received in final form 1st June 2004
Published online 7 September 2004 –

Abstract. The dynamics at a mesoscopic scale of the first-order magnetostructural transition in a $Gd_5(Si_xGe_{1-x})_4$ alloy with $x = 0.05$ is studied. We examine the effect of inducing the transition either by T or H on the entropy change. In addition, we analyse the avalanches between metastable states during the transition. The athermal character of the transition is evidenced. It is also shown that cycling through the transition leads to a reproducible pattern with no characteristic size of the avalanches.

PACS. 75.30.Sg Magnetocaloric effect, magnetic cooling – 75.30.Kz Magnetic phase boundaries – 64.70.Kb Solid-solid transitions

1 Introduction

There is renewed interest in using the magnetocaloric effect (MCE) as an alternative for refrigeration [1]. The MCE can be defined as the isothermal entropy change or the adiabatic temperature change arising from the application or removal of a magnetic field, H, in a magnetic system. The MCE may be maximised in the vicinity of a first-order phase transition, when the transformation is field-induced, resulting in a large contribution to the entropy change [1]. Such a giant MCE has been found in $Gd_5(Si_xGe_{1-x})_4$ compounds [2,3], in MnAs-based materials [4,5] and in $La(Fe_xSi_{1-x})_{13}$ alloys [6,7]. In this paper we study a $Gd_5(Si_xGe_{1-x})_4$ sample with $x = 0.05$. For this composition the first-order magnetostructural phase transition occurs from a high-temperature antiferromagnetic (AFM) Sm_5Ge_4-type orthorhombic phase to a low-temperature ferromagnetic (FM) Gd_5Si_4-type orthorhombic phase, at a transition temperature of $T_t \simeq 45$ K [3,8–10].

Differential scanning calorimeters (DSC) are particularly suited to the study of first-order structural phase transitions since they measure heat flow. Integration of the calibrated signal yields the latent heat, L, and the entropy change, ΔS, of the transition. Recently, we reported a new high-sensitivity DSC operating under magnetic field, H, [11] and showed that measurements sweeping T at a constant H yielded accurate values of ΔS at the first-order transition [12,13]. However, a direct evaluation of the MCE should be done while sweeping H at constant T. Our DSC is designed to operate in this sweeping-H mode. In the present paper, calorimetric results obtained by sweeping H and T are compared. Besides, calorimetric curves sweeping H through the transition reveal the discontinuous character of the transition dynamics which can be described in terms of avalanche events, whose analysis is also performed. Avalanches are associated with the nucleation and growth of domains of the new phase that take place during the first-order phase transition. Avalanche dynamics in phase transitions has been associated with many first-order phase transitions in disordered systems with athermal character [14]. In particular, it has been found in solids undergoing martensitic transformations (acoustic emission pulses) [15,16] and ferromagnets (Barkhausen noise) [17]. Recently, it has been suggested the martensitic nature of the irreversible AFM-to-FM transition occurring in Gd_5Ge_4 at low T [18]. Accordingly, burstlike effects may be present during the transformation [18].

The paper is organised as follows. In Section 2, experimental details are presented. In Section 3, calorimetric results of the entropy change are discussed. In Section 4, the dynamics of the transition is analysed. Finally, in Section 5 we summarise and conclude.

2 Experimental

$Gd_5(Si_xGe_{1-x})_4$ sample with $x = 0.05$ was synthesized by arc melting the pure elements in the desired stoichiometry under a high-purity argon atmosphere. The elements

[a] e-mail: amilcar@ffn.ub.es
[b] e-mail: xavier@ffn.ub.es

were placed in a water-cooled copper crucible and the resulting button was melted several times to ensure homogeneity. The weight losses after arc-melting were negligible. The as-prepared button was cut into rods, which were then treated for 9 h at 920 °C under 10^{-5} mbar, inside a quartz tube in an electrical resistance furnace. After annealing, the quartz tube was quickly taken out of the furnace and cooled to room temperature. The four rods are called V0, V1, V2 and V3. The crystallographic structure of the sample was studied by room-temperature X-ray diffraction (XRD). The sample displayed the expected room-temperature Sm_5Ge_4-type orthorhombic phase, in agreement with other studies [8,9]. Calorimetric measurements were performed using a high-sensitivity DSC specifically designed to study solid-solid phase transitions [11]. Heat flow $\dot{Q}(t)$, temperature $T(t)$ and magnetic field $H(t)$ were acquired at 0.25 Hz. Runs were performed within 4.2-300 K and 0-5 T in an LHe cryostat. Neither the thermometry nor the heat flow sensors were affected by H.

3 Measurement of the entropy change sweeping T and H

DSC are usually designed to sweep the temperature continuously while $\dot{Q}(t)$ and $T(t)$ are recorded. The sweeping-T mode induces the first-order transition in the sample, by releasing or absorbing heat. L and ΔS are given by:

$$L = \int_{T_s}^{T_f} \frac{dQ}{dT} dT \; ; \quad \Delta S_H = \int_{T_s}^{T_f} \frac{dQ}{dT} \frac{dT}{T} \; , \qquad (1)$$

where T_s and T_f are, respectively, temperatures above (below) and below (above) the start and finishing transition temperatures on cooling (heating). In the particular case of magnetostructural transitions, the transition temperature, T_t, shifts with the magnetic field [10]. Consequently, the field dependence of ΔS is obtained [11]. When operating in sweeping-H mode, the heat flow $\dot{Q}(t)$ and the field $H(t)$ are recorded. L and ΔS are thus given by:

$$L = \int_{H_s}^{H_f} \frac{dQ}{dH} dH \; ; \quad \Delta S_T = \frac{1}{T} \int_{H_s}^{H_f} \frac{dQ}{dH} dH = \frac{L}{T} \; , \qquad (2)$$

where H_s and H_f are, respectively, fields below (above) and above (below) the start and finishing transition fields on increasing (decreasing) the field.

For $x = 0.05$, curves at $T = 50$, 55, 60 and 65 K were measured (using sample V0). The transition field, H_t, which is evaluated as the field at the maximum of the dQ/dH curve, increases linearly with temperature, with a slope 5.0 ± 0.1 K/T. This value is in excellent agreement with those obtained from DSC sweeping T and magnetisation curves [10]. The entropy change at the transition increases with T, in agreement with the values obtained through DSC sweeping T (see Tab. 1). Curves at different field rates (0.1 and 1 T/min) for the same T yield the same values of L and ΔS within the experimental error, showing that measurements do not depend on the field rate.

Table 1. Entropy changes at a constant field, ΔS_H, and at constant temperature, ΔS_T, evaluated from DSC measurements sweeping the temperature and sweeping the field, respectively, in $Gd_5(Si_xGe_{1-x})_4$ with $x = 0.05$ (sample V0). The transition temperature, T_t, and the transition field, H_t, are also given. Values given for ΔS_T are the mean values of those obtained at rates of 0.1 and 1 T/min.

ΔS_H (J/kg K)				
	cooling		heating	
$\mu_0 H$ (T)	T_t (K)	ΔS	T_t (K)	ΔS
0	43.8	–14.57	46.5	14.29
1	49.4	–18.11	51.7	17.95
2	55.1	–23.04	57.1	22.00
3	60.2	–25.92	62.1	24.59
4	65.0	–27.86	66.6	26.77
5	69.1	–28.32	70.8	26.76
ΔS_T (J/kg K)				
	incr. H		decr. H	
T (K)	$\mu_0 H_t$ (T)	ΔS	$\mu_0 H_t$ (T)	ΔS
50	1.31	–14.81	0.94	10.36
55	2.16	–17.65	1.83	16.91
60	3.18	–20.96	2.85	18.19
65	4.29	-	3.93	-

The $H - T$ phase diagram for $x = 0.05$ is displayed in Figure 1. In this figure, H_t and T_t values as well as the onset and the end of the transitions are evaluated from DSC measurements sweeping H and T. The arrows in Figure 1 indicate examples of sweeping-T and sweeping-H transition paths along which the corresponding entropy changes, ΔS_H and ΔS_T, are measured. When the transition spreads in a field or temperature range, as is displayed in Figure 1, ΔS_H and ΔS_T might be different because initial and final states are distinct. This discrepancy between ΔS_H and ΔS_T can also be explained using general thermodynamics [19]. For a reversible process in a magnetic system

$$dE = dQ - MdH = TdS - MdH \; , \qquad (3)$$

where dE is the differential magnetic enthalpy and MdH is the differential external work done by the magnetic field. At a constant field, the sweeping-T path leads to an entropy change given by

$$\Delta S_H = \int_{T_s}^{T_f} \frac{dQ}{T} = \int_{T_s}^{T_f} \frac{dE_H}{T} \; . \qquad (4)$$

In contrast, along the sweeping-H path at constant temperature, the entropy change is written as

$$\Delta S_T = \frac{L}{T} = \frac{\Delta E_T}{T} + \frac{1}{T} \int_{H_s}^{H_f} MdH \; . \qquad (5)$$

In this case, the work done by the magnetic field over the system has to be considered. Only for an ideal transition, which occurs at a constant field and temperature, $(1/T) \int MdH$ vanishes and $\Delta S_T = \Delta S_H$.

For the studied sample, the evaluation of ΔS_T and ΔS_H leads to significantly different results. In particular,

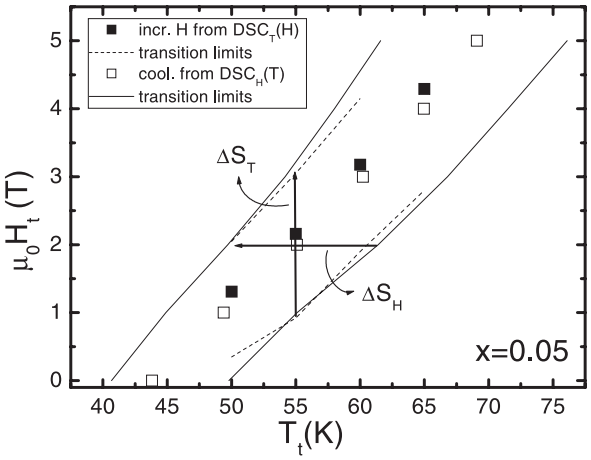

Fig. 1. $H-T$ phase diagram for $x = 0.05$, obtained from DSC measurements. $H_t(T)$ on increasing H (solid squares) and the corresponding start and finishing fields of the transition (dashed lines) are obtained sweeping H at constant T. $T_t(H)$ on cooling (open squares) and the corresponding start and finishing temperatures of the transition (solid lines) are obtained sweeping T at a constant H. Examples of the processes in which the entropy change is evaluated, are indicated with arrows.

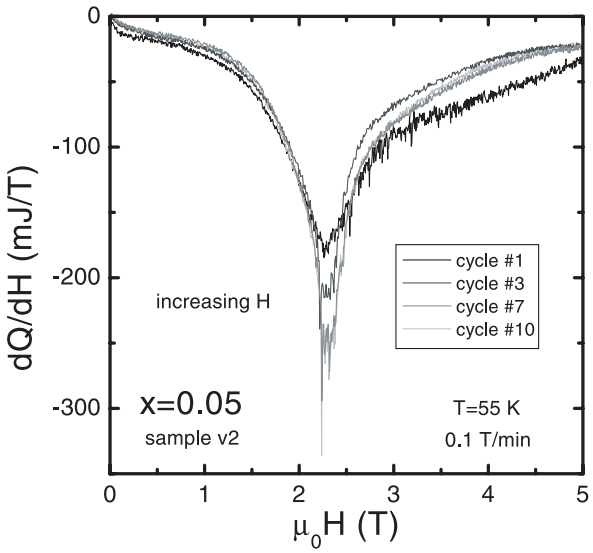

Fig. 2. Calorimetric curves recorded at $T = 55$ K on increasing H (0.1 T/min) for different cycles (#1, #3, #7 and #10, from top to bottom) for sample V2.

for sample V0, $\Delta S_H - \Delta S_T \sim 5$ J/kg K (see Tab. 1). Moreover, an estimation of $(1/T)\int_{H_s}^{H_f} MdH$ by using the $M(H)$ isotherm corresponding to the transition temperature [10] yields ~ 6.5 J/kg K. The agreement between the two values enables us to conclude that $\Delta E_T/T \approx \int dE_H/T$. Therefore, the values of the entropy change obtained by sweeping H or T are different due to the work needed to magnetise the system during the transition.

4 Dynamics of the magnetostructural transition

The calorimetric curves sweeping H, using a rate of 0.1 T/min [20], have similar shapes and collapse once they are normalised to $\dot{H}$. Interestingly, they reveal the jerky character of these transitions. This discontinuous behaviour is associated with the avalanche-type dynamics. Avalanches are the result of collective phenomena at a mesoscopic scale and are associated with the nucleation and growth of domains of the new structural phase that take place during the first-order phase transition. The nucleation can be thermally activated or athermal. In the first case, the relaxation from a metastable state may occur at constant external conditions due to thermal fluctuations, while in athermal transitions it occurs only when an external parameter (magnetic field, stress, temperature, etc.) changes, which modifies the difference of the free energy between the two phases [14,21].

When a system is driven externally through a first-order phase transition, it jumps from a given configuration —which is a state corresponding to a local minimum of the free energy— to a different configuration, once the local stability limit is reached. The path followed by the system depends on the presence of disorder such as dislocations, vacancies or grain boundaries, which controls the distribution of energy barriers separating the two phases. In the athermal case, the path can be reproduced from cycle to cycle provided that disorder does not evolve [14,21].

We have analysed the calorimetric curves when cycling repeatedly through the transition, for samples V1, V2 and V3 in the virgin state at the start of the measuring process. We consider that a cycle is the process followed by the system through the transition when the field is firstly sweeped to a maximum value and then decreased subsequently towards zero. From DSC curves obtained at constant T on increasing or decreasing H, the transformed fraction of a sample, y, can be evaluated as a function of H as

$$y(H) = \frac{1}{L}\int_{H_s}^{H} \frac{dQ}{dH} dH \ . \tag{6}$$

The curves $y(H)$ for increasing and decreasing H enable us to display the hysteresis loops. In order to quantify the amplitude of the jumps in the first-order transition (*i.e.*, structure peaks related to avalanches) present in $x = 0.05$ samples (see, for example, Figure 2 for sample V2), we computed the difference between two consecutive $y(H)$ values. This difference, Δy, which is a measurement of the size of the avalanches, can vary from 0 (no avalanche has occurred during the measuring time window) to 1 (the whole system undergoes the transition in a single avalanche). Figure 3 shows a histogram which is an approximation of the distribution of Δy, obtained from DSC measurement by increasing H at cycle 12 in sample V3.

The distribution of avalanches can be statistically analysed using the following probability distribution with two

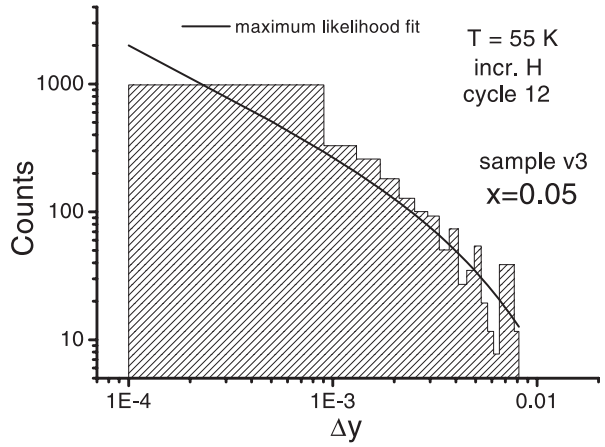

Fig. 3. Distribution of avalanches obtained from the difference in the transformed fraction (Δy) and the corresponding maximum likelihood fit for one of the measurements (cycle 12 increasing H) in sample V3.

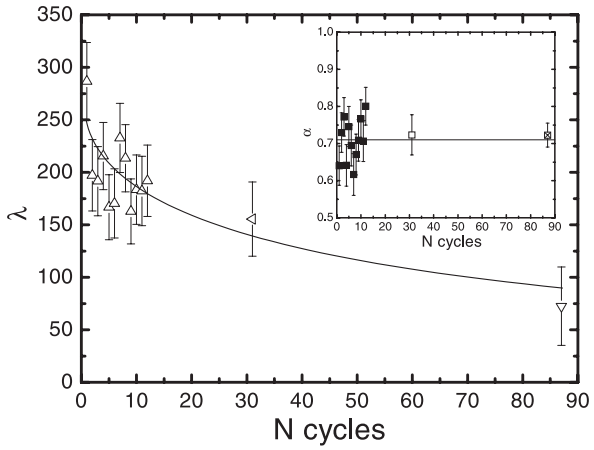

Fig. 4. Parameter λ obtained from the distribution of avalanches using the transformed fraction of the sample V3 ($x = 0.05$), as a function of the cycle, increasing H. Cycle 31 is taken from sample V2 and cycle 89 from sample V1. Inset: Exponent α obtained from the same distribution of avalanches. Solid lines are a guide to the eye.

free parameters (λ and α) [15,16]:

$$p(\Delta y) = \frac{e^{-\lambda \Delta y}(\Delta y)^{-\alpha}}{\int_{\Delta y_{min}}^{\Delta y_{max}} e^{-\lambda \Delta y}(\Delta y)^{-\alpha} d(\Delta y)} \; . \qquad (7)$$

For $\lambda = 0$, the distribution is power law [$p \propto (\Delta y)^{-\alpha}$, a critical behaviour where there is no characteristic size], while it is subcritical for $\lambda > 0$ (the distribution decays faster than a power law) and supercritical for $\lambda < 0$ (the distribution decays slower than a power law) [22]. $\Delta y_{min} = 10^{-4}$ is a value just above the intrinsic noise level of the measurements, evaluated by considering Δy values outside the region where the DSC peak shows structure. $\Delta y_{max} = 1$ is the maximum value.

From the calorimetric curve corresponding to the increasing-H process in a given cycle, we have estimated the exponent α and the parameter λ by the maximum likelihood method [23]. This method is the most reliable since it does not involve the computation of histograms, which normally depend on the binning choice. Figure 3 shows an example of one of such fits for sample V3. For this particular case, we obtain $\alpha = 0.80 \pm 0.05$ and $\lambda = 192 \pm 34$.

It has been reported for $Gd_5(Si_xGe_{1-x})_4$ that some properties vary when the transition is repeatedly induced. In particular, changes in the resistance [24,25] and thermopower [26] are reported for $Gd_5(Si_xGe_{1-x})_4$ alloys when they are thermally cycled through the transition. It is thus interesting to analyse the evolution of the dynamics of the transition with cycling. This evolution is clearly observed for all samples, since the shape of the first DSC cycle (increasing H) is different from subsequent cycles (see Fig. 2 for sample V2). Even at first glance it is obvious that the first measurement encloses a smaller area than the following measurements. The first cycle in sample V2 (see Fig. 2) shows small peaks of similar size. Some of them grow, while others diminish in subsequent cycles, reaching a reproducible distribution, which is characteristic of athermal transitions. A convenient approach is to follow the evolution of the avalanche distribution with cycling. Results from this study for increasing H in sample V3 are displayed in Figure 4. The parameter λ decreases with the number of cycles, while the exponent α (inset in Fig. 4) remains almost constant ($\alpha = 0.71 \pm 0.05$). We have also added the values fitted for the last cycle of sample V2 (cycle #31) and sample V1 (cycle #89), since those cycles were done with the same field rate as in sample V3. The latter values are in agreement with the behaviour of the two parameters for sample V3.

The evolution of the parameter λ suggests that $Gd_5(Si_xGe_{1-x})_4$ evolves from a subcritical distribution towards a power law distribution (where the system does not have a preferential avalanche size to undergo the transition), although the value $\lambda = 0$ is not reached in the 89th cycle. The characteristic exponent for the power law, α, presents a value ($= 0.71 \pm 0.05$) which depends neither on the evolution of the system with cycling nor on the sample. The evolution of the parameters is consistent with the direct observation of the DSC: when the system has chosen a path which is optimal to undergo the transition, the distribution of avalanches tends to be cycling independent.

5 Conclusions

The study of dynamics of the first-order transition in $Gd_5(Si_xGe_{1-x})_4$ alloys has revealed a very interesting behaviour. It has been found that the entropy change associated with the transition depends on whether it is field- or thermally-induced due to the work done by the magnetic field in the sweeping-H path. Besides, the jerky character of the calorimetric curves has been interpreted as a sequence of avalanches. The avalanche distribution evolves with cycling through the first-order transition. The structure of avalanches becomes repetitive after a few cycles tending towards a power-law distribution, evidencing the athermal character of the magnetostructural transition.

The financial support of the Spanish CICYT (MAT2003-01124 and MAT2001-3251) and Catalan DURSI (2001SGR00066) are recognized. FC and JM acknowledge DURSI for Ph.D. grants.

References

1. A.M. Tishin, Y.I. Spichkin, *The magnetocaloric effect and its applications* (Institute of Physics Publishing, Bristol and Philadelphia, 2003)
2. V.K. Pecharsky, K.A. Gschneidner, Jr., Phys. Rev. Lett. **78**, 4494 (1997)
3. V.K. Pecharsky, K.A. Gschneidner, Jr., Appl. Phys. Lett. **70**, 3299 (1997)
4. H. Wada, Y. Tanabe, Appl. Phys. Lett. **79**, 3302 (2001)
5. O. Tegus, E. Brück, K.H.J. Buschow, F.R. de Boer, Nature **415**, 450 (2002)
6. F.X. Hu, B.G. Shen, J.R. Sun, Z.H. Cheng, G.H. Rao, X.X. Zhang, Appl. Phys. Lett. **78**, 3675 (2001)
7. S. Fujieda, A. Fujita, K. Fukamichi, Appl. Phys. Lett. **81**, 1276 (2002)
8. V.K. Pecharsky, K.A. Gschneidner, Jr., J. Alloys Comp. **260**, 98 (1997)
9. L. Morellon, J. Blasco, P.A. Algarabel, M.R. Ibarra, Phys. Rev. B **62**, 1022 (2000)
10. F. Casanova, A. Labarta, X. Batlle, J. Marcos, Ll. Mañosa, A. Planes, S. de Brion, Phys. Rev. B **69**, 104416 (2004)
11. J. Marcos, F. Casanova, X. Batlle, A. Labarta, A. Planes, Ll. Mañosa, Rev. Sci. Inst. **74**, 4768 (2003)
12. F. Casanova, X. Batlle, A. Labarta, J. Marcos, Ll. Mañosa, A. Planes, Phys. Rev. B **66**, 100401(R) (2002)
13. F. Casanova, X. Batlle, A. Labarta, J. Marcos, Ll. Mañosa, A. Planes, Phys. Rev. B **66**, 212402 (2002)
14. F.J. Pérez-Reche, E. Vives, Ll. Mañosa, A. Planes, Phys. Rev. Lett. **87**, 195701 (2001)
15. E. Vives, J. Ortín, Ll. Mañosa, I. Ràfols, R. Pérez-Magrané, A. Planes, Phys. Rev. Lett. **72**, 1694 (1994)
16. L. Carrillo, Ll. Mañosa, J. Ortín, A. Planes, E. Vives, Phys. Rev. Lett. **81**, 1889 (1998)
17. R. Vergne, J.C. Cotillard, J.L. Porteseil, Rev. Phys. Appl. **16**, 847 (1981)
18. V. Hardy, S. Majumdar, S.J. Crowe, M.R. Lees, D.M. Paul, L. Hervé, A. Maignan, S. Hébert, C. Martin, C. Yaicle, M. Hervieu, B. Raveau, Phys. Rev. B **69**, 020407(R) (2004)
19. M.W. Zemansky, R.H. Dittman, *Heat and thermodynamics*, 6th ed. (McGraw-Hill, New York, 1981)
20. The rate $\dot{H} = 0.1$ T/min was optimal taking into account the sampling rate of the calorimeter, which is 0.25 Hz. This $\dot{H}$ enables us to observe the detailed structure of the calorimetric curve while the signal of the sensors is strong enough to be recorded above the noise
21. F.J. Pérez-Reche, M. Stipcich, E. Vives, Ll. Mañosa, A. Planes, M. Morin, Phys. Rev. B **69**, 064101 (2004)
22. E. Vives, A. Planes, Phys. Rev. B **50**, 3839 (1994)
23. R. Barlow, *Statistics* (Wiley, New York, 1989)
24. E.M. Levin, A.O. Pecharsky, V.K. Pecharsky, K.A. Gschneidner, Jr., Phys. Rev. B **63**, 064426 (2001)
25. J.B. Sousa, M.E. Braga, F.C. Correia, F. Carpinteiro, L. Morellon, P.A. Algarabel, M.R. Ibarra, Phys. Rev. B **67**, 134416 (2003)
26. J.B. Sousa, M.E. Braga, F.C. Correia, F. Carpinteiro, L. Morellon, P.A. Algarabel, M.R. Ibarra, J. Appl. Phys. **91**, 4457 (2002)